Inorganic Chemistry
Article

Inorg. Chem. **2011**, *50*, 1331–1338 **1331**
DOI: 10.1021/ic101945d

Osazone Anion Radical Complex of Rhodium(III)

Sarat Chandra Patra,[†] Manas Kumar Biswas,[†] Amarendra Nath Maity,[‡] and Prasanta Ghosh*[,†]

[†]*Department of Chemistry, R. K. Mission Residential College, Narendrapur, Kolkata-103, W.B., India, and*
[‡]*Department of Physics, National Dong Hwa University, Shou-Feng, Hualien 97401, Taiwan*

Received September 23, 2010

One electron paramagnetic parent osazone complex of rhodium of type *trans*-Rh($L^{NHPh}H_2$)(PPh_3)$_2Cl_2$ (**1**), defined as an osazone anion radical complex of rhodium(III), *trans*-Rh^{III}($L^{NHPh}H_2^{\bullet-}$)(PPh_3)$_2Cl_2$, $\mathbf{1}^{(t\text{-}RhL^{\bullet})}$, with a minor contribution (~2%) of rhodium(II) electromer, *trans*-Rh^{II}($L^{NHPh}H_2$)(PPh_3)$_2Cl_2$, $\mathbf{1}^{(t\text{-}Rh^{\bullet}L)}$, and their nonradical congener, *trans*-[Rh^{III}($L^{NHPh}H_2$)(PPh_3)$_2Cl_2$]I_3 ([*t*-**1**]$^+I_3^-$), have been isolated and are substantiated by spectra, bond parameters, and DFT calculations on equivalent soft complexes [Rh($L^{NHPh}H_2$)(PMe_3)$_2Cl_2$] (**3**) and [Rh($L^{NHPh}H_2$)(PMe_3)$_2Cl_2$]$^+$ (**3**$^+$). **1** is not stable in solution and decomposes to [*t*-**1**]$^+$ and a new rhodium(I) osazone complex, [Rh^I($L^{NHPh}H_2$)(PPh_3)Cl] (**2**). **1** absorbs strongly at 351 nm due to MLCT and LLCT, while [*t*-**1**]$^+$ and **2** absorb moderately in the range of 300−450 nm, respectively, due to LMCT and MLCT elucidated by TD-DFT calculations on $\mathbf{3}^{(t\text{-}RhL^{\bullet})}$, [*t*-**3**]$^+$, and Rh^I($L^{NHPh}H_2$)(PMe_3)Cl (**4**). EPR spectra of solids at 295 and 77 K, and dichloromethane−toluene frozen glass at 77 K of **1** are similar with $g = 1.991$, while $g = 2.002$ for the solid at 25 K. The EPR signal of **1** in dichloromethane solution is weaker ($g = 1.992$). In cyclic voltammetry, **1** displays two irreversible one electron transfer waves at +0.13 and −1.22 V, with respect to Fc^+/Fc coupling, due to oxidation of $\mathbf{1}^{(t\text{-}RhL^{\bullet})}$ to [*t*-**1**]$^+$ at the anode and reduction of rhodium(III) to rhodium(II), i.e., [*t*-**1**]$^+$ to electromeric $\mathbf{1}^{(t\text{-}Rh^{\bullet}L)}$ at the cathode.

Introduction

Osazone-assimilating nitrogen-enriched conjugated linkage (−HN−N=CH−CH=N−NH−) is a potential π-acidic NN-chelating agent that can augment stabilization of fascinating and reactive electronic states in coordination complexes. Electronic and molecular structures of the first transition metal complex of parent osazone ($L^{NHPh}H_2$) with a ruthenium(II) ion along with triphenyl phosphine (PPh_3) and chloride (Cl) as coligands as in *trans*-Ru^{II}($L^{NHPh}H_2$)(PPh_3)$_2Cl_2$ have recently been reported.[1] Bond parameters of the diimine fragment in conjunction with the density functional theory (DFT) calculations have authenticated the delocalization of significant electron density to the coordinated diimine fragment of the osazone in this ruthenium(II) complex. As compared to ruthenium, rhodium is one electron rich and has the possibility to localize the unpaired electron on rhodium or on the coordinated diimine fragment generating electro-isomers called electromers.[2] The electronic structure of the rhodium osazone complex incorporating PPh_3 and Cl ligands has been a subject of investigation here. In this article, the rhodium osazone complex of type *trans*-Rh($L^{NHPh}H_2$)(PPh_3)$_2Cl_2$ (**1**), its oxidized diamagnetic analogue *trans*-[Rh^{III}($L^{NHPh}H_2$)(PPh_3)$_2Cl_2$]I_3 ([*t*-**1**]$^+I_3^-$), and a rhodium(I) osazone complex of type Rh^I($L^{NHPh}H_2$)(PPh_3)Cl (**2**) have been reported. A rhodium osazone complex with molecular composition, Rh($L^{NHPh}H_2$)(PPh_3)$_2Cl_2$, can have the following electromers (Scheme 1).

In this article, the existence of an osazone anion radical complex, $\mathbf{1}^{(t\text{-}RhL^{\bullet})}$ with 2% spin density, is localized on the rhodium metal ion affording $\mathbf{1}^{(t\text{-}Rh^{\bullet}L)}$ in solids and solutions, and frozen glasses of **1** stabilized by two *trans* bulky PPh_3 ligands have been predicted.

Experimental Section

Hard and Soft Materials. All the physiochemical data have been collected on **1**, [*t*-**1**]$^+I_3^-$, and **2**, which are defined as hard materials. However, DFT or TD-DFT calculations at the B3LYP level of theory to analyze the spin density distributions (Figure 6), bond parameters (Chart 1), and transition probabilities (Table 5) have been performed on the model *cis* and *trans* isomers of Rh($L^{NHPh}H_2$)(PMe_3)$_2Cl_2$ (**3**), [Rh($L^{NHPh}H_2$)(PMe_3)$_2Cl_2$]$^+$ (**3**$^+$), and Rh($L^{NHPh}H_2$)(PMe_3)Cl (**4**), which are defined as soft materials.

Physical Measurements. Reagents or analytical grade materials were obtained from commercial suppliers and used without further purification. Spectroscopic grade solvents were used for spectroscopic and electrochemical measurements. The C, H, and N content of the compounds were obtained from a Perkin-Elmer 2400 series II elemental analyzer. Infrared spectra of the samples were measured from 4000 to 400 cm^{-1} with the KBr

*To whom correspondence should be addressed. E-mail: ghoshp_chem@yahoo.co.in. Phone: +91-33-2428-7017. Fax: +91-33-2477-3597.

(1) Roy, A. S.; Tuononen, H. M.; Rath, S. P.; Ghosh, P. *Inorg. Chem.* **2007**, *46*, 5942.

(2) Puschmann, F. F.; Harmer, J.; Stein, D.; Rüegger, H.; Bruin, B. D.; Grützmacher, H. *Angew. Chem., Int. Ed.* **2010**, *49*, 385–389 and relevant references there in.

Published on Web 01/24/2011

Scheme 1. Possible Electromers of $Rh(L^{NHPh}H_2)(PPh_3)_2Cl_2$

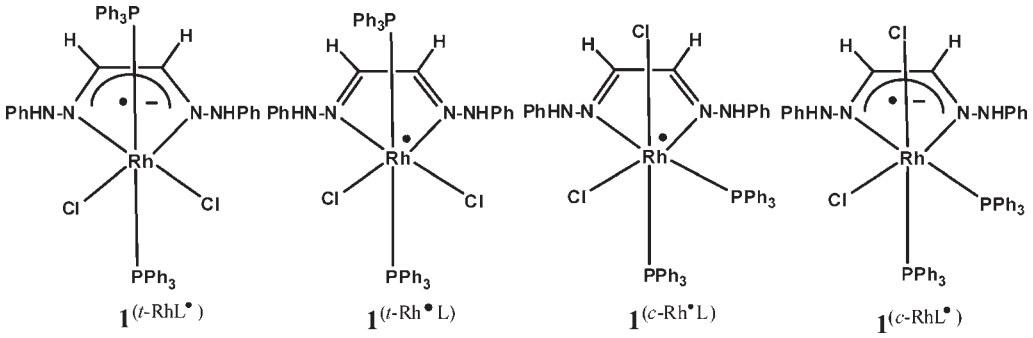

Table 1. Crystallographic Data for $[t\text{-}1]^+I_3^-$

chemical formula	$C_{50}H_{44}Cl_2I_3N_4P_2Rh$	T (K)	296(2)
fw	1317.34	ρ calcd (g cm^{-3})	1.778
space group	$P2/c$	reflns collected ($2\Theta_{max}$)	30578/52
a (Å)	12.0948(8)	unique reflns [$I > 2\sigma$ (I)]	4330/3149
b (Å)	13.6017(7)	no. of params/restr.	281/0
c (Å)	15.2096(8)	λ (Å/μ) (Mo, Kα) (cm^{-1})	0.71073/2.441
β (deg)	100.467(2)	R1[a] (GOF)[b]	0.0663/1.137
V (Å)	2460.5(2)	wR2[c] [I > 2σ (I)]	0.1743
Z	2	residual density (eÅ^{-3})	2.108

[a] Observation criterion: $R1 = \Sigma||F_o| - |F_c||/\Sigma|F_o|$. [b] Observation criterion: $GOF = \{\Sigma[w(F_o^2 - F_c^2)^2]/(n-p)\}^{1/2}$. [c] Observation criterion: $wR2 = \{\Sigma[w(F_o^2 - F_c^2)^2]/\Sigma[w(F_o^2)^2]\}^{1/2}$, where $w = 1/[\sigma^2(F_o^2) + (aP)^2 + bP]$, $P = (F_o^2 + 2F_c^2)/3$.

pellet at room temperature on a Perkin-Elmer Spectrum RX 1, FT-IR spectrophotometer. ^{1}H NMR spectra in DMSO-d_6 and $CDCl_3$ solvents were carried out on a Bruker DPX-300 MHz spectrometer. ESI mass spectra were recorded on a micro mass Q-TOF mass spectrometer. Electronic absorption spectra in solution at 298 K were carried out on a Perkin-Elmer Lambda 25 spectrophotometer in the range of 1100−200 nm. The X-band electron paramagnetic resonance (EPR) spectra were measured on a Bruker EMX spectrometer, where the microwave frequency was measured with a Hewlett-Packard 5246 L electronic counter. Magnetic susceptibility at 298 K has been measured on a Sherwood magnetic susceptibility balance. The electro-analytical instrument, BASi Epsilon-EC, has been used for cyclic voltammetric experiments and spectroelectrochemistry measurements.

Syntheses. Glyoxalbis(N-phenyl)osazone ($L^{NHPh}H_2$). This was prepared by the reported procedure.[1]

***trans*-Rh($L^{NHPh}H_2$)(PPh_3)$_2$Cl$_2$ (1).** To a hot solution of glyoxalbis-(N-phenyl)osazone ($L^{NHPh}H_2$) ligand (0.6 mmol) in absolute ethanol (30 mL), $RhCl_3$ (0.5 mmol) and PPh_3 (1.2 mmol) were added successively, and the reaction mixture was refluxed for 40 min (78 °C) under argon atmosphere. A red solid separated out. The solution mixture was cooled at 20 °C and filtered. The residue was dried in air and collected. Yield: 430 mg (∼ 92% with respect to rhodium). ESI (positive ion)-MS in CH_3CN; m/z: 936.83(**1**, calcd 936.68): Anal. Calcd for $C_{50}H_{44}Cl_2N_4P_2Rh$: C, 64.11; H, 4.73; N, 5.98. Found: C, 63.33; H, 4.44; N, 5.41. IR (KBr): ν = 3289 (m), 1599(s), 1493(vs), 1434(s), 1286(s), 1089(m), 744(s), 694(vs), and 519(vs) cm^{-1}.

***trans*-[Rh^{III}($L^{NHPh}H_2$)(PPh_3)$_2$Cl$_2$]I$_3$ ([*t*-1]$^+$I$_3^-$).** To a clear solution of **1** (100 mg, 0.1 mmol) in dichloromethane (30 mL), iodine (20 mg) in DCM (10 mL) was added slowly under argon, and the resulting solution mixture was kept at 25 °C. Red crystals of $[t\text{-}\mathbf{1}]^+I_3^-$ separated out from the reaction solution after 2−3 days, which were collected and used for single-crystal X-ray diffraction studies and other physiochemical measurements. Yield: 15 mg (12% with respect to **1**). ESI (positive ion)-MS in CH_3CN; m/z: 934.93 (**1**$^+$, calcd 936.68). Anal. Calcd for $C_{50}H_{44}Cl_2N_4P_2Rh^+I_3^-$: C, 45.58; H, 3.37; N, 4.25. Found: C, 45.34; H, 3.45; N, 4.11. ^{1}H NMR (DMSO-d_6, 300 MH, 295 K) δ (ppm) = 8.33 (s, 1H, N=CH), 7.77 (m, 9H, N=CH, Ph), 7.58 (m, 12H, Ph, and N=CH), 7.37 (m, 14H, Ph), 7.13 (t, 3H, Ph), 7.10 (d, 1H, Ph), 6.05 (d, 2H, Ph). IR (KBr): ν = 3289 (m), 1600(m), 1492(m), 1437(s), 1190(s), 1120 (vs), 722(vs), 694(vs), and 542(vs) cm^{-1}.

Rh^I($L^{NHPh}H_2$)(PPh_3)Cl (2). Sample **1** (200 mg, 0.2 mmol) was stirred in dichloromethane for 10 h at 295 K. The solution was then filtered off ,and the filtrate was evaporated under vacuum. A red solid was obtained, which was thoroughly washed with boiling hexane to remove PPh_3 as one of the products. The desired product, **2**, was isolated after purification of the crude mass on a basic alumina column and using $CHCl_3$ as the eluent. Yield: 50 mg (∼36% with respect to **1**). ESI (positive ion)-MS in CH_3CN; m/z: 637.20 (**2**, calcd 638.95). Anal. Calcd for $C_{32}H_{29}ClN_4PRh$: C, 60.15; H, 4.57; N, 8.77. Found: C, 60.95; H, 4.25; N, 8.32. ^{1}H NMR ($CDCl_3$, 300 MH, 295 K) δ (ppm) = 8.28 (s, 2H, NH), 7.99 (s, 2H, N=CH), 7.79 (d, 6H, PPh_3), 7.67 (m, 4H, Ph, PPh_3), 7.5 (m, 7H, PPh_3), 7.09 (t, 4H, Ph), 6.96 (t, 2H, Ph), 6.01 (d, 2H, Ph). IR (KBr): ν = 3277(m), 1599(m), 1559(m), 1540(m), 1490(m), 1436(m), 1260(m), 1088(s), 744(s), 692(vs), and 518(vs) cm^{-1}.

X-ray Crystallographic Data Collection and Refinement of the Structure. A dark brown single crystal of $[t\text{-}\mathbf{1}]^+I_3^-$ was picked and mounted on a Bruker APEX-II CCD diffractometer equipped with a Mo-target rotating-anode X-ray source and a graphite monochromator (Mo-Kα, λ = 0.71073 Å). Final cell constants were obtained from least-squares fits of all measured reflections. The structure was readily solved by direct method and subsequent difference Fourier techniques. The crystallographic data of $[t\text{-}\mathbf{1}]^+I_3^-$ is listed in Table 1. ShelX97[3] was used for the structure solution and refinement. All non-hydrogen atoms were refined anisotropically. Hydrogen atoms were placed at calculated positions and refined as riding atoms with isotropic displacement parameters.

Density Functional Theory (DFT) Calculations. All calculations reported in this article were done with the Gaussian 03W[4]

(3) (a) Sheldrick, G. M. *ShelXS97*; Universität Göttingen: Göttingen, Germany, 1997. (b) Sheldrick, G. M. *ShelXL97*; Universität Göttingen: Göttingen, Germany, 1997.

program package supported by GaussView 4.1. The DFT[5] and TD-DFT[6] calculations have been performed at the level of Becke three parameter hybrid functional with the nonlocal correlation functional of Lee−Yang−Parr (B3LYP).[7] The gas phase geometries of *cis* and *trans* isomers of $Rh(L^{NHPh}H_2)(PMe_3)_2Cl_2$ (**3**), $[Rh(L^{NHPh}H_2)(PMe_3)_2Cl_2]^+$ (**3**$^+$), and $Rh(L^{NHPh}H_2)(PMe_3)Cl$ (**4**) have been optimized on theoretical coordinates using Pualy's Direct Inversion[8] in the Iterative Subspace (DIIS), using the "tight" convergent SCF procedure[9] ignoring symmetry. In all calculations, a LANL2DZ basis set, along with the corresponding effective core potential (ECP), was used for rhodium metal.[10−12] Valence double-ζ basis set, 6-31G[13] for H was used. For C, N, P, and Cl non-hydrogen atoms valence double-ζ plus diffuse and polarization functions, 6-31++G**[14] as basis set were employed for the calculations. The percentage contribution of ligand and metal to the frontier orbitals of **3**, **3**$^+$, and **4** have been calculated using the GaussSum program package.[15] The 60 lowest singlet excitation energies on the optimized geometries of **3**, **3**$^+$, and **4** in dichloromethane using the CPCM model[16] have been elucidated with the TD-DFT method.

Results and Discussion

Syntheses. The dark red compound, *trans*-$Rh(L^{NHPh}H_2)(PPh_3)_2Cl_2$ (**1**), stable in solid state, has been synthesized in high yield (90% with respect to Rh) by reacting $RhCl_3$ with PPh_3 and the osazone ligand ($L^{NHPh}H_2$) in boiling ethanol under anaerobic condition. **1** is one electron paramagnetic (μ_{eff} = 1.70 μ_B), and the spin is mostly localized on the osazone ligand forming the $\mathbf{1}^{(t\text{-RhL}\bullet)}$ electromer. **1** is not stable and even under argon slowly produces *trans*-$[Rh^{III}(L^{NHPh}H_2)(PPh_3)_2Cl_2]^+$, $[t\text{-}\mathbf{1}]^+$, and a rhodium(I) osazone complex, $Rh^I(L^{NHPh}H_2)(PPh_3)Cl$ (**2**). Formation of products, $[t\text{-}\mathbf{1}]^+$ and **2** from **1** indicates in solution the contribution of $\mathbf{1}^{(t\text{-Rh}\bullet\text{L})}$ electromer, which is a rhodium(II) osazone complex that undergoes facile disproportionation reaction[17] to a rhodium(III) osazone complex, $[t\text{-}\mathbf{1}]^+$ and **2**, a new square planar rhodium(I) osazone complex as eq 1. Upon chromatographic separation, **2** has been isolated as a pure product. As the electromers, $\mathbf{1}^{(t\text{-RhL}\bullet)}$ and $\mathbf{1}^{(t\text{-Rh}\bullet\text{L})}$ are very reactive in solution, and they undergo oxidation affording a $[t\text{-}\mathbf{1}]^+$ cation in the presence of any kind of oxidizing agent as in eq 2. Oxidation of **1** by I_2 in dichloromethane under argon affords the crystals of $[t\text{-}\mathbf{1}]^+I_3^-$ in low yield (∼12% with respect to **1**).

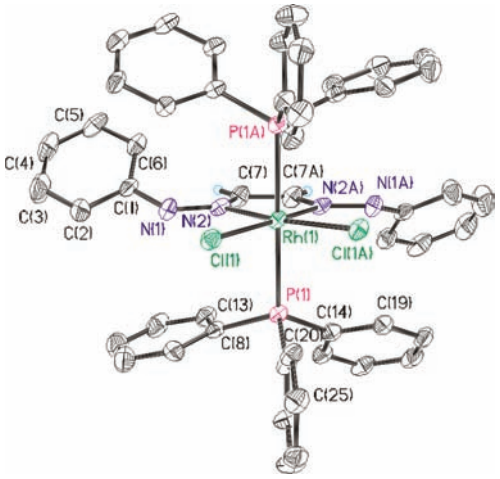

Figure 1. Molecular structure of the $[t\text{-}\mathbf{1}]^+$ in crystals of $[t\text{-}\mathbf{1}]^+I_3^-$ (I_3^- ion is omitted for clarity).

$$2\,\mathbf{1}^{(t\text{-Rh}\bullet\text{L})} \rightarrow [t\text{-}\mathbf{1}]^+ + \mathbf{2} + PPh_3 + Cl^- \quad (1)$$

$$\mathbf{1}^{(t\text{-RhL}\bullet)} \rightarrow [t\text{-}\mathbf{1}]^+ + e \quad (2)$$

All of these compounds (**1**, $[t\text{-}\mathbf{1}]^+I_3^-$, and **2**) have been characterized by elemental analyses and various spectra including the single crystal X-ray structure determination of $[t\text{-}\mathbf{1}]^+I_3^-$. In IR spectra, the NH stretching frequency appears at 3289, 3289, and 3277 cm^{-1} for **1**, $[t\text{-}\mathbf{1}]^+I_3^-$, and **2**, respectively.

Molecular Geometry in Crystals. $[t\text{-}\mathbf{1}]^+I_3^-$. Single crystal X-ray structure determination of $[t\text{-}\mathbf{1}]^+I_3^-$ has confirmed the molecular geometry of $[\mathbf{1}]^+$ in crystals. It crystallizes in space group $P2/c$. The molecular structure

(4) Frisch, M. J.; Trucks, G. W.; Schlegel, H. B.; Scuseria, G. E.; Robb, M. A.; Cheeseman, J. R.; Montgomery, Jr., J. A.; Vreven, T.; Kudin, K. N.; Burant, J. C.; Millam, J. M.; Iyengar, S. S.; Tomasi, J.; Barone, V.; Mennucci, B.; Cossi, M.; Scalmani, G.; Rega, N.; Petersson, G. A.; Nakatsuji, H.; Hada, M.; Ehara, M.; Toyota, K.; Fukuda, R.; Hasegawa, J.; Ishida, M.; Nakajima, T.; Honda, Y.; Kitao, O.; Nakai, H.; Klene, M.; Li, X.; Knox, J. E.; Hratchian, H. P.; Cross, J. B.; Bakken, V.; Adamo, C.; Jaramillo, J.; Gomperts, R.; Stratmann, R. E.; Yazyev, O.; Austin, A. J.; Cammi, R.; Pomelli, C.; Ochterski, J. W.; Ayala, P. Y.; Morokuma, K.; Voth, G. A.; Salvador, P.; Dannenberg, J. J.; Zakrzewski, V. G.; Dapprich, S.; Daniels, A. D.; Strain, M. C.; Farkas, O.; Malick, D. K.; Rabuck, A. D.; Raghavachari, K.; Foresman, J. B.; Ortiz, J. V.; Cui, Q.; Baboul, A. G.; Clifford, S.; Cioslowski, J.; Stefanov, B. B.; Liu, G.; Liashenko, A.; Piskorz, P.; Komaromi, I.; Martin, R. L.; Fox, D. J.; Keith, T.; Al-Laham, M. A.; Peng, C. Y.; Nanayakkara, A.; Challacombe, M.; Gill, P. M. W.; Johnson, B.; Chen, W.; Wong, M. W.; Gonzalez, C.; Pople, J. A. *Gaussian 03*, Revision E.01; Gaussian, Inc.: Wallingford CT, 2004.
(5) (a) Hohenberg, P.; Kohn, W. *Phys. Rev.* **1964**, *136*, B864. (b) Kohn, W.; Sham, L. J. *Phys. Rev.* **1965**, *140*, A1133. (c) Parr, R. G.; Yang, W. *Density Functional Theory of Atoms and Molecules*; Oxford University Press: Oxford, U.K., 1989. (d) *The Challenge of d and f Electrons*; Salahub, D. R., Zerner, M. C., Eds.; ACS Symposium Series 394; American Chemical Society: Washington, D.C., 1989.
(6) (a) Bauernschmitt, R.; Haser, M.; Treutler, O.; Ahlrichs, R. *Chem. Phys. Lett.* **1996**, *256*, 454. (b) Stratmann, R. E.; Scuseria, G. E.; Frisch, M. *J. Chem. Phys.* **1998**, *109*, 8218. (c) Casida, M. E.; Jamoroski, C.; Casida, K. C.; Salahub, D. R. *J. Chem. Phys.* **1998**, *108*, 4439.
(7) (a) Becke, A. D. *J. Chem. Phys.* **1993**, *98*, 5648. (b) Lee, C.; Yang, W.; Parr, R. G. *Phys. Rev. B* **1988**, *37*, 785. (c) Miehlich, B.; Savin, A.; Stoll, H.; Preuss, H. *Chem. Phys. Lett.* **1989**, *157*, 200.
(8) Pulay, P. *J. Comput. Chem.* **1982**, *3*, 556.
(9) Schlegel, H. B.; McDouall, J. J. *Computational Advances in Organic Chemistry*, Ogretir, C.; Csizmadia, I. G., Eds.; Kluwer Academic: The Netherlands, 1991, pp 167−185.
(10) Hay, P. J.; Wadt, W. R. *J. Chem. Phys.* **1985**, *82*, 270.
(11) Wadt, W. R.; Hay, P. J. *J. Chem. Phys.* **1985**, *82*, 284.
(12) Hay, P. J.; Wadt, W. R. *J. Chem. Phys.* **1985**, *82*, 299.
(13) (a) Hehre, W. J.; Ditchfield, R.; Pople, J. A. *J. Chem. Phy.* **1972**, *56*, 2257. (b) Hariharan, P. C.; Pople, J. A. *Theo. Chim. Acta* **1973**, *28*, 213. (c) Hariharan, P. C.; Pople, J. A. *Mol. Phys.* **1974**, *27*, 209. (d) Rassolov, V. A.; Ratner, M. A.; Pople, J. A.; Redfern, P. C.; Curtiss, L. A. *J. Comput. Chem.* **2001**, *22*, 976. (e) Francl, M. M.; Pietro, W. J.; Hehre, W. J.; Binkley, J. S.; DeFrees, D. J.; Pople, J. A.; Gordon, M. S. *J. Chem. Phys.* **1982**, *77*, 3654.
(14) (a) Hariharan, P. C.; Pople, J. A. *Theo. Chim. Acta* **1973**, *28*, 213. (b) Clark, T.; Chandrasekhar, J.; Spitznagel, G. W.; Schleyer, P. V. R. *J. Comput. Chem.* **1983**, *4*, 294.
(15) O'Boyle, N. M.; Tenderholt, A. L.; Langner, K. M. *J. Comput. Chem.* **2008**, *29*, 839.
(16) (a) Cossi, M.; Rega, N.; Scalmani, G.; Barone, V. *J. Comput. Chem.* **2003**, *24*, 669. (b) Barone, V.; Cossi, M. *J. Phys. Chem. A* **1998**, *102*, 1995.
(17) (a) Paul, P.; Tyagi, B; Bilakhiya, A. K.; Bhadhade, M. M.; Suresh, E. *Dalton Trans.* **1999**, 2009–2014. (b) Brown, G. M.; Chan, S. F.; Creutz, C.; Schwartz, H. A.; Sutin, N. *J. Am. Chem. Soc.* **1979**, *101*, 7638. (c) Mulazzani, Q. G.; Emmi, S.; Hoffman, M. Z.; Venturi, M. *J. Am. Chem. Soc.* **1981**, *103*, 3362. (d) Schwarz, H. A.; Creutz, C. *Inorg. Chem.* **1983**, *22*, 707. (e) Kew, G.; DeArmond, K.; Hanck, K. *J. Phys. Chem.* **1974**, *78*, 727. (f) Kew, G.; Hanck, K.; DeArmond, K. *J. Phys. Chem.* **1975**, *79*, 1828.

Table 2. Selected Bond Distances (Å) and Angles (deg) of $[t\text{-}\mathbf{1}]^+I_3^-$

Rh(1)−Cl(1)	2.356(19)
Rh(1)−P(1)	2.409(18)
Rh(1)−N(2)	2.033(6)
N(1)−N(2)	1.339(8)
N(1)−C(1)	1.404(9)
N(2)−C(7)	1.319(10)
C(7)-C(7A)	1.403(16)
N(2)−N(1)−C(1)	127.4(7)
C(7)−N(2)−N(1)	123.4(6)
C(6)−C(1)−N(1)	122.8(7)
N(2)−C(7)−C(7A)	116.9(4)

with the atom numbering scheme is depicted in Figure 1, and the relevant bond parameters are summarized in Table 2. In crystals of $[t\text{-}\mathbf{1}]^+I_3^-$, two bulky triphenyl phosphine ligands are *trans* to each other. The average Rh(1)−P(1) and Rh(1)−Cl(1) distances are 2.4090(18) and 2.3556(19) Å, respectively. The corresponding Ru^{II}−P and Ru^{II}−Cl distances in *trans*-$Ru^{II}(L^{NHPh}H_2)(PPh_3)_2Cl_2$ are 2.3718(8) and 2.4421(8) Å, respectively. Both Rh(III) and Ru(II) are t_{2g}^6 metal ions but the effective nuclear charge (Z_{eff}*) of Rh(III) ion is higher than that of Ru(II) ion. The metal ion with the higher Z_{eff}*, will expectedly result in shorter M−Cl bonds (σ bonding) but longer M−PPh_3 bonds (π bonding) as observed in Rh(III)−Cl and Rh(III)−PPh_3 length trends (Rh(III)−Cl < Ru(II)−Cl and Rh(III)−PPh_3 > Ru(II)−PPh_3).

Bond parameters of the osazone ligand in $[t\text{-}\mathbf{1}]^+I_3^-$, as given in Chart 1a are of importance to analyze the electronic structure of the complex. The =CH−CH= bond of the diimine fragment is shorter than the expected length of two sp^2 hybridized carbon atoms (1.47 Å), but two −N=C− bonds are longer than a normal −N=C− bond (1.28 Å). In $[t\text{-}\mathbf{1}]^+I_3^-$, the average −N=C− and =CH−CH= bond lengths are 1.319(6) and 1.403(16) Å, respectively. These bond parameters of the −HN−N=CH−CH=N−NH− fragment correlate well to those reported in the first osazone complex, $Ru^{II}(L^{NHPh}H_2)(PPh_3)_2Cl_2$[1] (Chart 1b), and are consistent with the neutral diimine description as established in other neutral diimine species reported by Raston et al.[18] and Wieghardt et al.[19] The N−N distance in $[t\text{-}\mathbf{1}]^+I_3^-$ is 1.339(8) Å. Thus, the $[t\text{-}\mathbf{1}]^+$ ion has been described as an osazone complex of rhodium(III) ion, and the trend of such bond parameters has been investigated by DFT calculations.

EPR Spectra. The solid state EPR spectra of **1** at 295, 77, and 25 K have been recorded. The EPR spectra of **1** in dichloromethane at 295 and 310 K and dichloromethane−toluene frozen glass at 77 K have also been recorded. All the spectra are shown in Figures 2 and 3.

(18) (a) Cloke, F. G. N.; Dalby, C. I.; Henderson, M. J.; Hitchcock, P. B.; Kennard, C. H. L.; Lamb, R. N.; Raston, C. L. *J. Chem. Soc., Chem. Commun.* **1990**, 1394. (b) Cloke, F. G. N.; Hanson, G. R.; Henderson, M. J.; Hitchcock, P. B.; Kennard, C. H. L.; Raston, C. L. *J. Chem. Soc., Chem. Commun.* **1989**, 1002. (c) Gardiner, M. G.; Hanson, G. R.; Henderson, M. J.; Lee, F. C.; Raston, C. L. *Inorg. Chem.* **1994**, *33*, 2456.

(19) (a) Ghosh, P.; Bill, E.; Bothe, E.; Weyhermüller, T.; Neese, F.; Wieghardt, K. *J. Am. Chem. Soc.* **2003**, *125*, 1293. (b) Muresan, N.; Chlopek, K.; Weyhermüller, T.; Neese, F.; Wieghardt, K. *Inorg. Chem.* **2007**, *46*, 5327. (c) Muresan, N.; Lu, C. C.; Ghosh, M.; Peters, J. C.; Abe, M.; Henling, L. M.; Weyhermüller, T.; Bill, E.; Wieghardt, K. *Inorg. Chem.* **2008**, *47*, 4579. (d) Ghosh, M.; Sproules, S.; Weyhermueller, T.; Wieghardt, K. *Inorg. Chem.* **2008**, *47*, 5963. (e) Ghosh, M.; Weyhermüller, T.; Wieghardt, K. *Dalton Trans.* **2008**, 5149.

Chart 1. (a) Experimental Bond Lengths of Osazone in $[t\text{-}\mathbf{1}]^+I_3^-$, with Corresponding Calculated Lengths of $[t\text{-}\mathbf{3}]^+$ in Parentheses. (b) Experimental Bond Lengths of Osazone in *trans*-$Ru^{II}(L^{NHPh}H_2)(PPh_3)_2Cl_2$ (ref 1). (c) Calculated Lengths of Osazone in $\mathbf{3}^{(t\text{-RhL}\bullet)}$ Electromer. (d) Calculated Lengths of Osazone in **4**

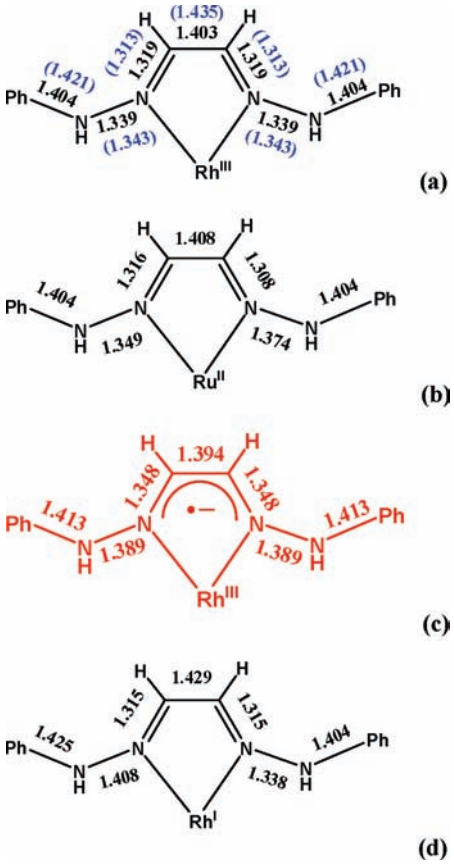

No signal has been detected at 310 K in dichloromethane solution. The *g* parameter for the measurements in frozen glasses at 77 K and solid (room 295 and 77 K) is 1.991, which is 2.002 at 25 K for solids. In dichloromethane solution at 295 K, although the paramagnetic signal is weaker, it appears at $g = 1.992$ (Figure 2). All these data are consistent with the presence of a single paramagnetic center, i.e., one pure electromer in the bulk sample of **1**. The deviation from the $g = 2.004$ may be due to localization of some amount of spin density on the metal center having the $\mathbf{1}^{(t\text{-Rh}\bullet\text{L})}$ electromer. But at 25 K, the *g* value is 2.002, prompting that the electron is more localized on the osazone ligand.

The high energy difference between $\mathbf{3}^{(t\text{-RhL}\bullet)}$ and $\mathbf{3}^{(c\text{-RhL}\bullet)}$ electromers does not support the presence of equilibrium mixture of *trans* and *cis* electromers localizing 2% and 4% spin density on the rhodium ion as shown in Figure 6. But the mixing of $\mathbf{1}^{(t\text{-RhL}\bullet)}$ with the excited state (LUMO), where the electron is localized more on the rhodium metal ion can broaden the spectrum more. The possibility of transition has been noted in cyclic voltammetry study and LMCT bands in the electronic spectra of **1**. The EPR spectral features and instabilities of **1** in solution at room temperature thus can be well explained by the presence of a low percentage of $\mathbf{1}^{(t\text{-Rh}\bullet\text{L})}$ with the electromer, $\mathbf{1}^{(t\text{-RhL}\bullet)}$. $\mathbf{1}^{(t\text{-Rh}\bullet\text{L})}$ is a rhodium(II) compound and disproportionates spontaneously to $[t\text{-}\mathbf{1}]^+$ and **2** as observed experimentally and in other reported complexes.[17]

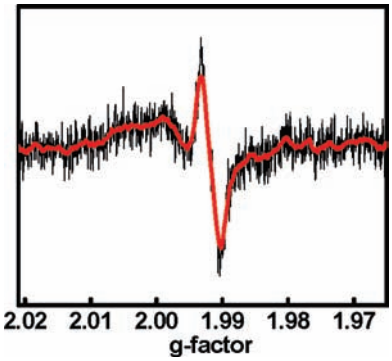

Figure 2. X-band EPR spectrum of **1** in dichloromethane at 295 K (red line denotes the average plot; frequency, 9.446 GHz; modulation amplitude, 5.0 G).

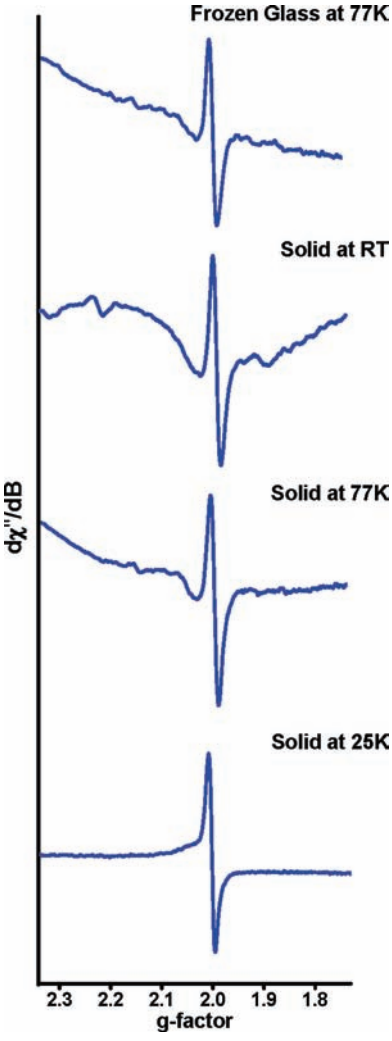

Figure 3. X-band EPR spectra of **1** in frozen glass (dichloromethane) at 77 K and solid at 295, 77, and 25 K (frequency, 9.132−9.433 GHz).

Gas Phase Geometries and Electronic Structures of 1, 1^+, and 2. Gas phase geometries and bond parameters of **1** and $\mathbf{1}^+$ have been investigated by density functional theory (DFT) calculations on model compounds $Rh(L^{NHPh}H_2)(PMe_3)_2Cl_2$ (**3**) and $[Rh(L^{NHPh}H_2)(PMe_3)_2Cl_2]^+$ ($\mathbf{3}^+$). Geometries of both *cis* and *trans* isomers of **3** have been optimized with doublet spin state to identify the most stable electromer. Geometries of both *cis* and *trans* isomers of $\mathbf{3}^+$ have also been optimized with singlet spin state to compare the stabilities (Figure 4). The calculated bond parameters of significant isomers have been summarized in Table 3. The calculation shows that the *trans* isomer of $\mathbf{3}^+$, abbreviated as $[t\text{-}\mathbf{3}]^+$, is stabilized by 35.6 KJ/mol compared to the *cis* isomer, $[c\text{-}\mathbf{3}]^+$. The closed shell singlet (CSS) solution of *trans*-isomer of $[t\text{-}\mathbf{3}]^+$ satisfactorily reproduces the experimental bond parameters of the osazone ligand of $[t\text{-}\mathbf{1}]^+I_3^-$. Because of the replacement of PPh_3 by PMe_3, the calculated bond parameters of the coordination sphere of $[t\text{-}\mathbf{3}]^+$ are comparatively higher than those found in $[t\text{-}\mathbf{1}]^+I_3^-$ experimentally (Tables 1 and 3). The CSS solution has no instability due to triplet perturbations rejecting the possibility of having diradical singlet (S = 0) as the ground state. The features of unexpected longer −C═N and shorter = CH−CH= distances as given in Chart 1(a) are due to the mixing of the $\pi_{diimine}$* of the osazone ligand with the filled d-orbital of the Rh(III) ion. One such case is shown in Figure 5, which is defined as d → $\pi_{diimine}$* back bonding that results in transfer of a metal electron to the LUMO of osazone as observed in *trans*-$Ru^{II}(L^{NHPh}H_2)(PPh_3)_2Cl_2$.[1]

Table 3. Calculated Bond Parameters of the Coordination Sphere for $\mathbf{3}^{(t\text{-}RhL\bullet)}$, $[t\text{-}\mathbf{3}]^+$, and **4** at the B3LYP Level of the Theory

average	$[t\text{-}\mathbf{3}]^+$	**4**	$\mathbf{3}^{(t\text{-}RhL\bullet)}$
Rh−Cl	2.405	2.411	2.459
Rh−P	2.432	2.304	2.417
Rh−N	2.085	2.076	2.073

DFT calculations on *trans* and *cis* isomers of **3** show that in both cases, the electron density is localized on the osazone ligand generating $\mathbf{3}^{(t\text{-}RhL\bullet)}$ and $\mathbf{3}^{(c\text{-}RhL\bullet)}$ types of electromers, respectively, as depicted in Figure 6. Similar to the order of higher stabilities of *trans* isomers $[t\text{-}\mathbf{3}]^+$ compared to the *cis* isomer $[c\text{-}\mathbf{3}]^+$ of $[\mathbf{3}]^+$ ion, the *trans* electromer, $\mathbf{3}^{(t\text{-}RhL\bullet)}$ is more stable than the *cis* electromer, $\mathbf{3}^{(c\text{-}RhL\bullet)}$ by 64 KJ/mol, excluding the possibility of existence of $\mathbf{3}^{(c\text{-}RhL\bullet)}$ in solid or solution.

The calculated bond parameters of the coordination sphere of $\mathbf{3}^{(t\text{-}RhL\bullet)}$ are listed in Table 3. The bond parameters of the osazone fragment (Chart 1c) are remarkably different from those obtained from single crystal X-ray structure determinations and DFT calculations on $[t\text{-}\mathbf{1}]^+I_3^-$ and *trans*-$Ru^{II}(L^{NHPh}H_2)(PPh_3)_2Cl_2$ as given in Chart 1b. The comparatively much longer −C═N− (1.348 Å), N−N (1.389 Å), and shorter =CH−CH= (1.394 Å) bond length trends of the osazone moiety of the optimized structure of $\mathbf{3}^{(t\text{-}RhL\bullet)}$ correlate well to those found in the diimine anion radical complexes.[18−20] Mulliken spin population analyses have shown that spin density is mostly localized on the diimine fragment of the osazone ligand with around 2% only on the rhodium ion (Figure 6), correlating well with the EPR spectra . Thus, compound **1** here has been defined as the first osazone anion radical complex of type $\mathbf{1}^{(t\text{-}RhL\bullet)}$ with around 2% contribution of rhodium(II) osazone electromer, $\mathbf{1}^{(t\text{-}Rh\bullet L)}$, as shown in Scheme 1. The calculation has shown that formation of osazone anion radical lengthens the Rh−Cl bond (Table 3) *trans* to an imine nitrogen, where a significant amount of spin density is localized.

(20) Bailey, P. J.; Dick, C. M.; Fabre, S.; Parsons, S.; Yellowlees, L. J. *Dalton Trans.* **2006**, 1602.

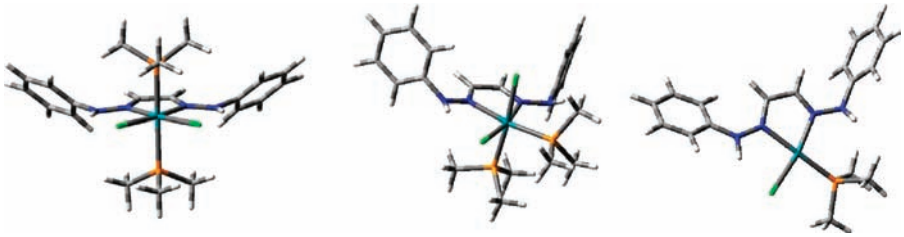

Figure 4. Optimized geometries of $[t\text{-}\mathbf{3}]^+$, $[c\text{-}\mathbf{3}]^+$, and **4**.

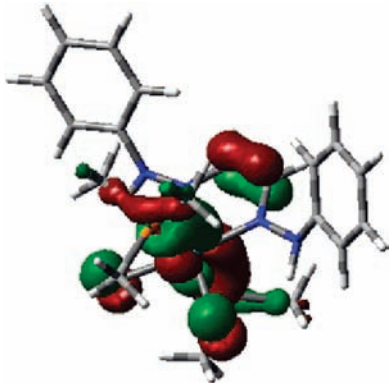

Figure 5. Mixing of filled d_{Rh} with $\pi_{diimine^*}$ of $L^{NHPh}H_2$.

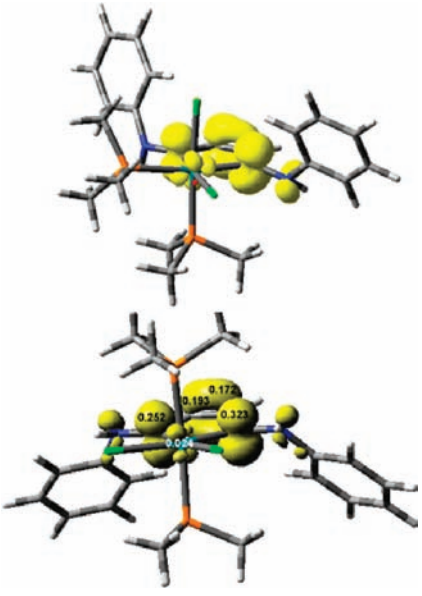

Figure 6. Mulliken spin density plot of $\mathbf{3}^{(t\text{-}RhL\bullet)}$ (bottom) and $\mathbf{3}^{(c\text{-}RhL\bullet)}$ (top) as derived from UB3LYP/DFT.

To elucidate the trend of bond parameters of the osazone in **2**, the gas-phase geometry of $Rh(L^{NHPh}H_2)(PMe_3)Cl$ (**4**) has been optimized (Figure 4), and relevant bond parameters are listed in Table 3 and Chart 1d. The calculated bond parameters of **4** are very similar to those found in $[t\text{-}\mathbf{1}]^+I_3^-$, $[t\text{-}\mathbf{3}]^+$, and *trans*-$Ru^{II}(L^{NHPh}H_2)(PPh_3)_2Cl_2$ (Chart 1) and are consistent with the presence of a neutral osazone ligand coordinated to rhodium(I) in **2**.

Cyclic Voltammetry Study and Electronic Spectra. The electron transfer events of **1** in dichloromethane solution under a completely N_2-atmosphere have been studied by

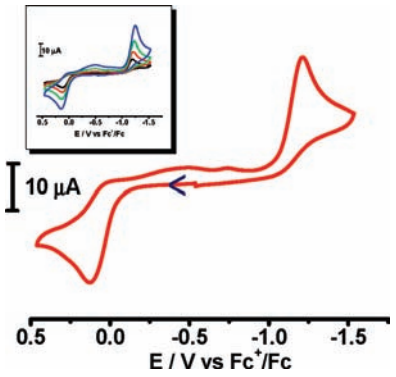

Figure 7. Cyclic voltammogram of **1** in CH_2Cl_2 at 295 K (conditions: 0.1(M) $[N(n\text{-}Bu)_4]PF_6$ supporting electrolyte; scan rates 50 (black), 100 (red), 200 (green), and 400 (blue) mV s^{-1}; glassy carbon working electrode).

cyclic voltammetry, which displays two irreversible one electron transfer waves at +0.13 and −1.22 V with respect to the Fc^+/Fc couple as shown in Figure 7. The anodic peak at 0.13 V has been assigned to the oxidation of the osazone anion radical to osazone, i.e., $\mathbf{1}^{(t\text{-}RhL\bullet)}$ to $[t\text{-}\mathbf{1}]^+$, while the cathodic peak at −1.22 V has been assigned to the reduction of rhodium(III) to rhodium(II), i.e., $[t\text{-}\mathbf{1}]^+$ to $\mathbf{1}^{(t\text{-}Rh\bullet L)}$. The Rh^{III}/Rh^{II} reduction potential (−1.22 V with respect to the Fc^+/Fc couple) of **1** is comparable to those reported in other rhodium(III)−heterocyclic diimine or pyridyl complexes.[17e,f,21,22]

The event is noteworthy and is a phenomenon of electro-isomerism.[2] It explains the stability of the cation in solution that has been isolated successfully by oxidizing $\mathbf{1}^{(t\text{-}RhL\bullet)}$ with an I_2 solution. The large shift of the potential of this redox couple (1.35 V, 130 KJ/mol for one electron transfer) is due to the transfer of the electron from the anion ligand to the metal, transforming rhodium(III) to rhodium(II) in a similar geometrical feature. The transformation of $\mathbf{1}^{(t\text{-}RhL\bullet)}$ to $\mathbf{1}^{(t\text{-}Rh\bullet L)}$ is costly and correlates well with the HOMO to LUMO excitation energies in **3** (in dichloromethane). HOMO is composed of $L^{NHPh}H_2$ (100%), while the LUMO is composed of Rh+Cl orbitals (75%) and $L^{NHPh}H_2$ (25%). The calculated HOMO to LUMO excitation energy is 97 kJ/mol, but for a LUMO with no contribution of $L^{NHPh}H_2$, the excitation energy is expected to be 129 kJ/mol that is very similar to the experimental voltage shift of 1.35 V during the reduction process of $[t\text{-}\mathbf{1}]^+/\mathbf{1}$ couple in dichloromethane solution.

(21) Gonzalez, V.; Adams, H.; Thomas, J. A. *Dalton Trans.* **2005**, 110–115.
(22) Amarante, D.; Cherian, C.; Catapano, A.; Adams, R.; Wang, M. H.; Megehee, E. G. *Inorg. Chem.* **2005**, *44*, 8804–8809.

The electronic spectra of **1**, $[t\text{-}\mathbf{1}]^+$, and **2** in dichloromethane solutions are characteristic and are shown in Figure 8. Data have been summarized in Table 4. Compound **1** absorbs strongly at 352 nm with a shoulder at 443 nm. The absorption features of $[t\text{-}\mathbf{1}]^+$ and **2** at 300−440 nm are different. To elucidate the origins of absorptions of all these complexes, TD-DFT calculations have been carried out on **3**, $[t\text{-}\mathbf{3}]^+$, and $Rh(L^{NHPh}H_2)(PMe_3)Cl$ (**4**). For each compound, 60 lowest singlet excitation energies on the optimized geometries in dichloromethane have been elucidated using a conductor-like polarizable continuum (CPCM) model. Calculated energies, significant contributions, transitions types, and dominant contributions of these three calculations are listed in Table 5.

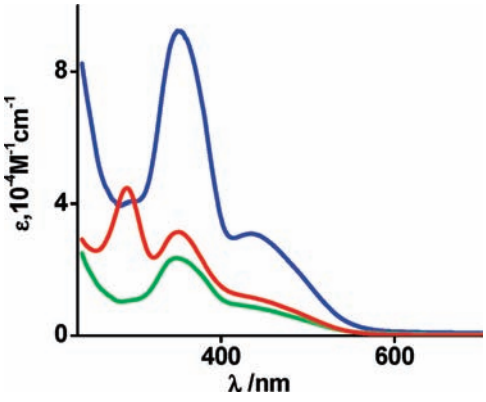

Figure 8. Electronic spectra of **1** (blue), $[t\text{-}\mathbf{1}]^+I_3^-$ (red), and **2** (green) in dichloromethane at 295 K.

Table 4. Electronic Spectral Data of **1**, $[t\text{-}\mathbf{1}]^+I_3^-$, and **2** in Dichloromethane

complexes	λ_{max}, nm (ε, 10^4 $M^{-1}cm^{-1}$)
1	443 (3.1), 352 (9.3)
$[t\text{-}\mathbf{1}]^+I_3^-$	446 (1.2), 350 (3.2), 291(4.4)
2	448(0.9), 347(2.4)

Calculations have shown that for the rhodium(III) osazone complex, $[t\text{-}\mathbf{3}]^+$, all the significant absorptions above 300 nm are due to ligand-to-metal charge transfers (LMCT), while for the rhodium(I) osazone complex, **4**, the significant absorptions are due to metal-to-ligand charge transfer (MLCT). The radical complex **3** has mixed origins, i.e., LMCT, LLCT, and MLCT. The high-intensity transition at 351.2 nm for compound **3** involves following electrons transfers: alpha HOMO (based on the singly occupied $\pi_{diimine}$* orbital of the osazone) → high lying ligand based α LUMO+8 and LUMO+10; β HOMO-3 (based on the rhodium(III) d-orbital) → LUMO (based on the unoccupied $\pi_{diimine}$* orbital of the osazone); and HOMO-2 (based on the rhodium(III) d-orbital) → LUMO (based on the unoccupied $\pi_{diimine}$* orbital of the osazone). Thus, the strong absorption band at 352 nm of **1** has been assigned to LLCT and MLCT origins.

Calculations have further shown the origins of the low-energy absorption band of **1** and $[t\text{-}\mathbf{1}]^+$ at higher than 440 nm. Calculations for **3** find an absorption band at 553.9 nm because of the transition of the electron from the beta HOMO (based on the $\pi_{diimine}$ of the osazone) to LUMO (based on the $\pi_{diimine}$* of the osazone), while the band at 456.7 nm is due to the transitions from alpha HOMO-1 ($\pi_{diimine}$ of the osazone) to the LUMO (based on the rhodium(III) d-orbital) and beta HOMO ($\pi_{diimine}$ of the osazone) to LUMO+1 (based on the rhodium(III) d-orbital). Experimentally, no significant absorption band above 500 nm has been observed in the complex of **1**, but the low-energy band at around 440 nm of **1** has been assigned to a LMCT band. Similarly for $[t\text{-}\mathbf{3}]^+$, the

Table 5. Calculated Excitation Energies with Oscillator Strength and Significant Transitions of **3**, $[t\text{-}\mathbf{3}]^+$, and **4**

λ/nm (f)	exp. λ	significant contributions	transition type	dominant contribution
		3		
553.9 (0.088)		β HOMO → LUMO (93%)	$\pi_L \rightarrow \pi^*_L$	LLCT
456.7 (0.037)	443	α HOMO-1 → LUMO (46%)	$\pi_L \rightarrow d_{Rh(III)} + \pi^*_L$	LMCT
		β HOMO → LUMO +1 (25%)	$\pi_L \rightarrow d_{Rh(III)} + \pi^*_L$	LMCT
372.0 (0.127)		α HOMO-2 → LUMO (41%)	$\pi_L \rightarrow d_{Rh(III)} + \pi^*_L$	LMCT
		α HOMO → LUMO+6 (10%)	$\pi_L \rightarrow \pi^*_L$	LLCT
		β HOMO-1 → LUMO+1 (26%)	$\pi_L \rightarrow d_{Rh(III)} + \pi^*_L$	LMCT
351.2 (0.145)	352	α HOMO → LUMO+8 (17%)	$\pi_L \rightarrow \pi^*_L$	LLCT
		α HOMO → LUMO+10 (14%)	$\pi_L \rightarrow \pi^*_L + p_P$	LLCT
		β HOMO-3 → LUMO (12%)	$d_{Rh(III)} + \pi_L + p_{Cl} \rightarrow \pi^*_L$	MLCT
		β HOMO-2 → LUMO (22%)	$d_{Rh(III)} + p_{Cl} \rightarrow \pi^*_L$	MLCT
335.9 (0.022)		α HOMO → LUMO+8 (28%)	$\pi_L \rightarrow d_{Rh(III)}$	LMCT
		β HOMO-2 → LUMO (21%)	$d_{Rh(III)} + p_{Cl} \rightarrow \pi^*_L$	MLCT
		$[t\text{-}\mathbf{3}]^+$		
446.8 (0.133)	446	HOMO-6 → LUMO (48%)	$\pi_L \rightarrow \pi^*_L$	LLCT
		HOMO → LUMO+1 (26%)	$\pi_L \rightarrow d_{Rh(III)} + \pi^*_L + p_{Cl}$	LMCT
438.9 (0.033)		HOMO → LUMO+2 (72%)	$\pi_L \rightarrow d_{Rh(III)} + p_P$	LMCT
427.6 (0.426)		HOMO → LUMO+1 (48%)	$\pi_L \rightarrow d_{Rh(III)} + \pi^*_L + p_{Cl}$	LMCT
342.1 (0.039)	350	HOMO-2 → LUMO+1 (62%)	$\pi_L + p_{Cl} + p_P \rightarrow d_{Rh(III)} + \pi^*_L + p_{Cl}$	LMCT
		HOMO-1 → LUMO+1 (36%)	$\pi_L + p_{Cl} + p_P \rightarrow d_{Rh(III)} + \pi^*_L + p_{Cl}$	LMCT
317.5 (0.047)		HOMO-5 → LUMO+1 (80%)	$\pi_L \rightarrow d_{Rh(III)} + \pi^*_L + p_{Cl}$	LMCT
		4		
434.5 (0.243)	448	HOMO-3 → LUMO (41%)	$d_{Rh} \rightarrow \pi^*_L$	MLCT
		HOMO-2 → LUMO (33%)	$d_{Rh} \rightarrow \pi^*_L$	MLCT
403.66 (0.532)	347	HOMO-3 → LUMO (33%)	$d_{Rh} \rightarrow \pi^*_L$	MLCT
		HOMO-2 → LUMO (47%)	$d_{Rh} \rightarrow \pi^*_L$	MLCT

absorption band at 446.8 nm has origins of LLCT and LMCT, while the band at 438.9 is purely a LMCT band. Thus, the calculations have established that LMCT is the origin of the low-energy absorption bands of **1** and $[t\text{-}\mathbf{1}]^+$ around 440 nm.

Conclusion

The first osazone anion radical ($L^{NHPh}H_2^{\bullet-}$) coordinated to a rhodium(III) ion as in the *trans*-$Rh^{III}(L^{NHPh}H_2^{\bullet-})(PPh_3)_2Cl_2$, $\mathbf{1}^{(t\text{-}RhL\bullet)}$ electromer, a major component (~98%) of the paramagnetic *trans*-$Rh(L^{NHPh}H_2)(PPh_3)_2Cl_2$ (**1**) complex, has been authenticated by experimental and theoretical studies. EPR parameters and DFT calculations have predicted a minor contribution (~2%) of the rhodium(II) electromer, *trans*-$Rh^{II}(L^{NHPh}H_2)(PPh_3)_2Cl_2$, $\mathbf{1}^{(t\text{-}Rh\bullet L)}$, in **1**. The bond parameters of the osazone anion radical and spectral features of $\mathbf{1}^{(t\text{-}RhL\bullet)}$ have been compared with its decomposed nonradical analogues, [*trans*-$Rh^{III}(L^{NHPh}H_2)(PPh_3)_2Cl_2$], $[t\text{-}\mathbf{1}]^+$, and $Rh^I(L^{NHPh}H_2)(PPh_3)Cl$ (**2**). In cyclic voltammetry, $\mathbf{1}^{(t\text{-}RhL\bullet)}$ to $[t\text{-}\mathbf{1}]^+$ oxidation at the anode and $[t\text{-}\mathbf{1}]^+$ to $\mathbf{1}^{(t\text{-}Rh\bullet L)}$ reduction at the cathode generating electromeric species have been assigned. The study has established that osazone is redox non-innocent, and with transition metal ions, osazone can generate electromeric species. Elucidation of molecular and electronic structures of those electron transfer states appears to be worth investigation.

Acknowledgment. We thank UGC (F. No. 34-315/2008 (SR) and DST (SR/S1/IC- 10/2008), New Delhi for financial support.

Supporting Information Available: Crystallographic data in CIF format for $[t\text{-}\mathbf{1}]^+I_3^-$. These materials are available free of charge via the Internet at http://pubs.acs.org.